Interseismic Plate coupling and strain partitioning in the Northeastern Caribbean

D. M. Manaker,[1]* E. Calais,[1] A. M. Freed,[1] S. T. Ali,[1] P. Przybylski,[1]
G. Mattioli,[2] P. Jansma,[2] C. Prépetit[3] and J. B. de Chabalier[4]

[1]*Purdue University, Department of Earth and Atmospheric Sciences, West Lafayette,* IN 47907, *USA. E-mail: ecalais@purdue.edu*
[2]*University of Arkansas, Department of Geosciences, Fayetteville, AK, USA*
[3]*Bureau of Mines and Energy, Port-au-Prince, Haiti*
[4]*Institut de Physique du Globe, Laboratoire de Sismologie, Paris, France*

SUMMARY

The northeastern Caribbean provides a natural laboratory to investigate strain partitioning, its causes and its consequences on the stress regime and tectonic evolution of a subduction plate boundary. Here, we use GPS and earthquake slip vector data to produce a present-day kinematic model that accounts for secular block rotation and elastic strain accumulation, with variable interplate coupling, on active faults. We confirm that the oblique convergence between Caribbean and North America in Hispaniola is partitioned between plate boundary parallel motion on the Septentrional and Enriquillo faults in the overriding plate and plate-boundary normal motion at the plate interface on the Northern Hispaniola Fault. To the east, the Caribbean/North America plate motion is accommodated by oblique slip on the faults bounding the Puerto Rico block to the north (Puerto Rico subduction) and to the south (Muertos thrust), with no evidence for partitioning. The spatial correlation between interplate coupling, strain partitioning and the subduction of buoyant oceanic asperities suggests that the latter enhance the transfer of interplate shear stresses to the overriding plate, facilitating strike-slip faulting in the overriding plate. The model slip rate deficit, together with the dates of large historical earthquakes, indicates the potential for a large (M_w7.5 or greater) earthquake on the Septentrional fault in the Dominican Republic. Similarly, the Enriquillo fault in Haiti is currently capable of a M_w7.2 earthquake if the entire elastic strain accumulated since the last major earthquake was released in a single event today. The model results show that the Puerto Rico/Lesser Antilles subduction thrust is only partially coupled, meaning that the plate interface is accumulating elastic strain at rates slower than the total plate motion. This does not preclude the existence of isolated locked patches accumulating elastic strain to be released in future earthquakes, but whose location and geometry are not resolvable with the present data distribution. Slip deficit on faults from this study are used in a companion paper to calculate interseismic stress loading and, together with stress changes due to historical earthquakes, derive the recent stress evolution in the NE Caribbean.

Key words: Space geodetic surveys; Subduction zone processes; Kinematics of crustal and mantle deformation.

GJI Seismology

1 INTRODUCTION

Oblique plate motion at subduction zones is often associated with the partitioning of strain between trench-normal convergence at the plate interface and trench-parallel strike-slip in the overriding plate, usually near the volcanic arc. Examples are widespread, including subduction of the Indian Plate beneath Sumatra (McCaffrey 1991; Prawirodirdjo *et al.* 1997), the Pacific Plate beneath the Aleutians (Ave Lallemant & Oldow 2000), the Cocos Plate beneath Central America (DeMets 2001; La Femina *et al.* 2002) and the North American Plate beneath Hispaniola (Calais *et al.* 2002).

Strain partitioning is generally assumed to occur if shear stresses in the overriding plate are large enough to activate strike-slip faulting (Bowman *et al.* 2003). High plate convergence obliquity has

*Now at: BP, 501 Westlake Park Blvd., Houston, TX, USA.

been proposed as one of the factors that promotes partitioning by increasing the amount of shear stress available in the overriding plate (Fitch 1972; McCaffrey 1992). Strong interplate coupling (Beck 1983; Jarrard 1986) or high friction on the subduction interface (Chemenda *et al.* 2000) have also been shown to enhance the transfer of shear stresses to the overriding plate, thereby facilitating strain partitioning. If this is true, then lateral variations in interplate coupling along an oblique subduction zone should correlate with variations in the degree of strain partitioning.

Thanks to dense geodetic networks at subduction plate boundaries, we now understand that interseismic deformation in the upper plate involves the combination of secular block rotations (possibly with internal deformation) and strain accumulation on a plate interface with laterally variable coupling (Prawirodirdjo *et al.* 1997; McCaffrey 2002, 2005; Wallace *et al.* 2005). Such variations have been correlated by some with the occurrence of large earthquakes (Ruff & Kanamori 1980, 1983; Scholz & Campos 1995), with the premise that rupture areas of great earthquakes correspond to large, continuous and strongly coupled regions of subduction plate interfaces that resist applied stresses. The mapping of lateral variation of interplate coupling at subduction zones is therefore critical to better understand the mechanical behaviour of the seismogenic zone, with fundamental implications for assessing hazards associated with megathrust earthquakes.

Oblique subduction in the northeastern Caribbean shows a rare example of along-strike transition from a fully partitioned (Hispaniola) to non-partitioned (Puerto Rico) plate motion, in spite of a similar convergence obliquity (Fig. 1; Mann *et al.* 2002; ten Brink & Lin 2004). Interestingly, the transition coincides with the subduction of the buoyant Bahamas platform under Hispaniola, whereas normal oceanic lithosphere descends beneath Puerto Rico. This

transition also coincides with the rupture area of the 1946–1953 sequence of *M*7.0 to *M*8.1 earthquakes (Dolan & Wald 1998).

The northeastern Caribbean provides a natural laboratory to investigate strain partitioning, its causes and its consequences on the stress regime and tectonic evolution of a subduction plate boundary. In this paper, we use a GPS velocity field covering the northeastern Caribbean to map the degree of interseismic coupling at the Caribbean–North America oblique subduction interface and estimate slip rates on major active faults. This will serve to test whether the transition from a partitioned to non-partitioned kinematics mentioned above corresponds to a transition from locked to unlocked oblique subduction interface. In addition our kinematic model provides long-term (secular) strain and inferred stress rates that, combined with short-term co- and postseismic stresses, allows for the calculation of Coulomb stress changes and the investigation of the distribution of large earthquakes in space and time as a function of the evolution of crustal stresses (Ali *et al.* 2008).

2 DATA AND MODELLING METHODOLOGY

2.1 GPS velocity field

The GPS velocity field is derived from data collected at campaign and continuous GPS sites from 1994 to 2005 in Haiti, the Dominican Republic, Puerto Rico, the Virgin Islands and the Lesser Antilles. We processed phase and pseudo-range GPS data using the GAMIT software (version 10.2; King & Bock 2005), solving for station coordinates, satellite state vectors, seven tropospheric delay parameters per site and day and phase ambiguities using double-differenced GPS phase measurements. We used the final orbits from
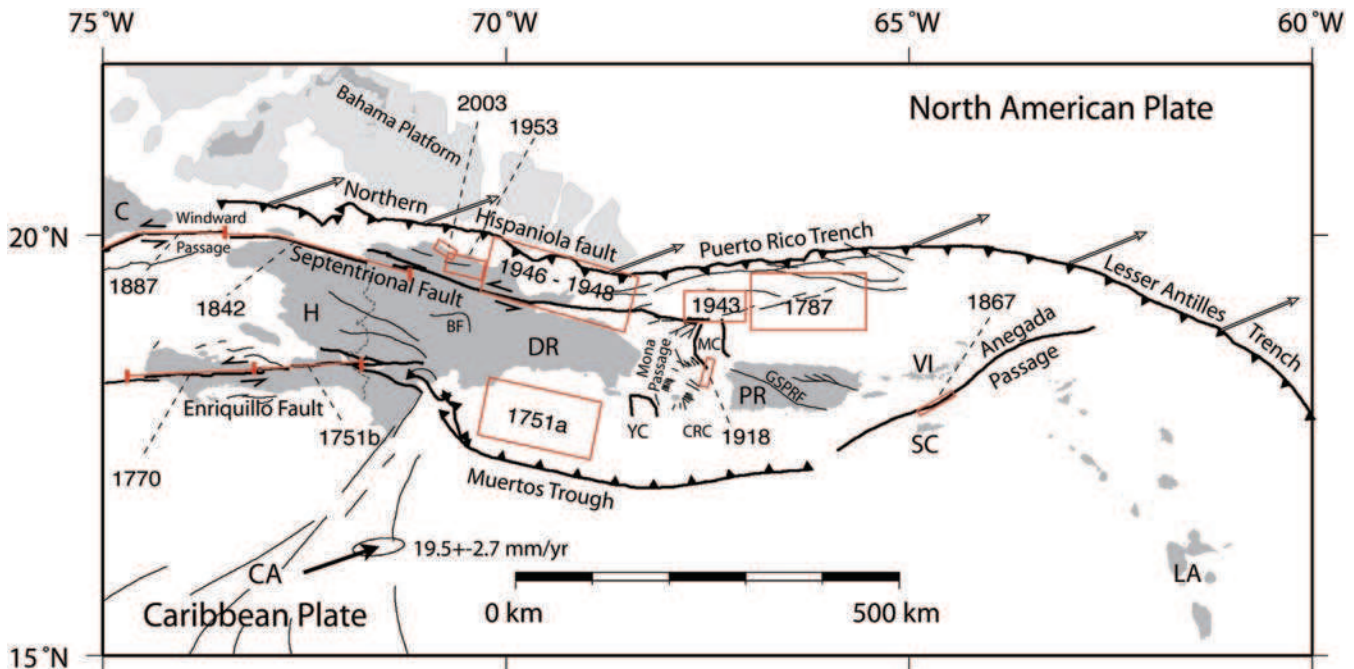
Figure 1. Major features of Northeastern Caribbean. Black lines indicate regional faults and fault systems. Heavy lines represent major faults that are modelled in this study. Black arrow labelled (CA) and white arrows along the subduction thrust show velocity of the Caribbean plate relative to the North American Plate, based on DeMets *et al.* (2000). Large earthquakes since 1564 are shown by red countour boxes that represent the surface projection of hypothetical rupture areas. Note the clustering of events in the since 1900 in the region between Hispaniola (H + DR) and Puerto Rico (PR). Fault segments with red bars at either end show hypothetical rupture length on vertical faults. Geographical abbreviations are C, Cuba; H, Haiti; DR, Dominican Republic; PR, Puerto Rico; LA, Lesser Antilles; CRC, Cabo Rojos Canyon; YC, Yuma Canyon; SC, St Croix; MC, Mona Canyon; GSPRF, Great Southern Puerto Rico Fault; BF Bonao Fault.
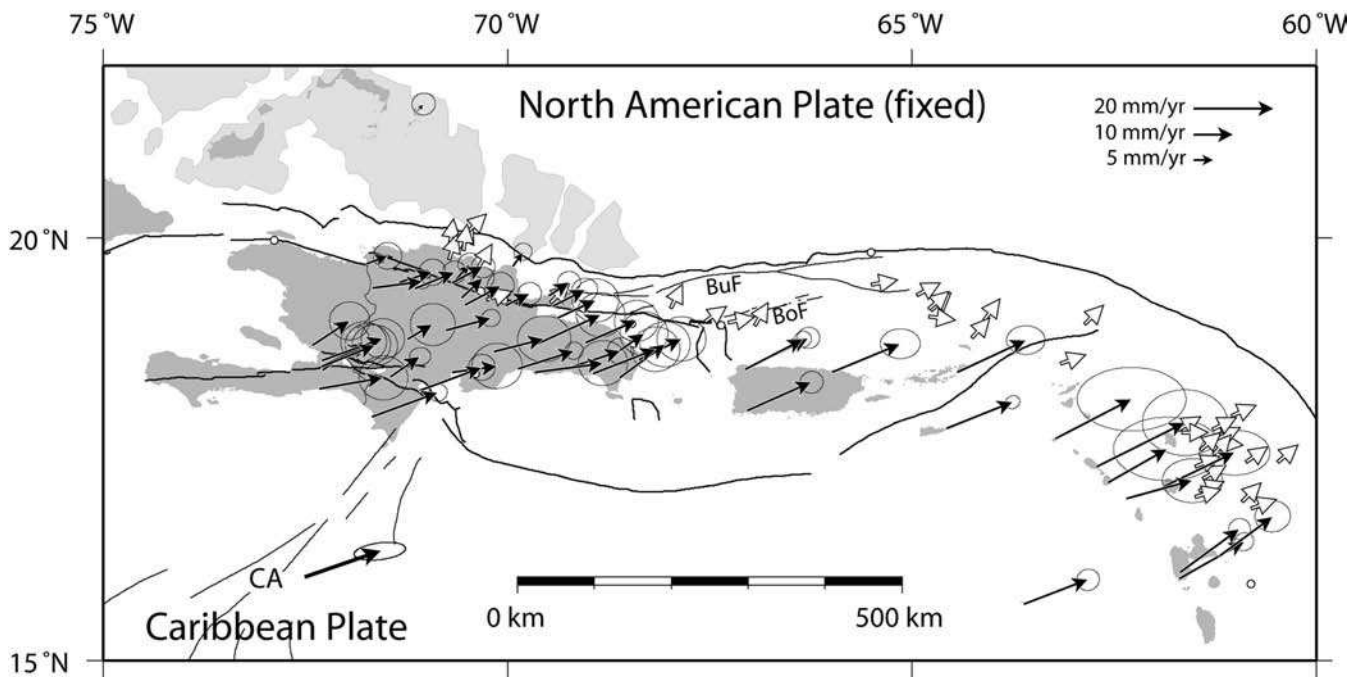
Figure 2. GPS velocities used in this study, shown by black arrows. Ellipses are 95 per cent confidence. The heavy black arrow (CA) shows the velocity of the Caribbean plate relative to the North American Plate, from DeMets *et al.* (2000). White arrows show the earthquake slip vectors used in this study. BoF, Bowin Fault; BuF, Bunce fault.

the International GNSS Service (IGS), earth orientation parameters from the International Earth Rotation Service (IERS) and applied azimuth- and elevation-dependent antenna phase centre models, following the tables recommended by the IGS. We included 15 global IGS stations in North America, South America and the Caribbean to serve as ties with the International Terrestrial Reference Frame (ITRF2000, Altamimi *et al.* 2002).

The least-squares adjustment vector and its corresponding variance-covariance matrix for station positions and orbital elements estimated for each independent daily solution were then combined with global solution independent exchange format (SINEX) files from the IGS daily processing routinely done at the Scripps Orbital and Permanent Array Center (http://sopac.ucsd.edu). The reference frame is implemented using this unconstrained combined solution by minimizing the position and velocity deviations of 41 IGS core stations with respect to the ITRF2000 while estimating an orientation and translation transformation. In this process, height coordinates were downweighted using a variance scaling factor of 10 compared with the horizontal components. We then rotate ITRF2000 station velocities into a North America-fixed reference frame by removing the rigid rotation of the North American Plate defined by Calais *et al.* (2006). Long-term baseline repeatabilities are of the order of 2–4 mm for horizontal components and 5–10 mm for the vertical component. Velocity uncertainties are of the order of 2–3 mm yr^{-1} at one standard deviation for most stations, allowing daily stochastic variations of site coordinates of 0.5 mm^2 d^{-1} to account for a noise model that combines white and random-walk noise.

Pollitz & Dixon (1998) suggest that the postseismic transient signal due to relaxation of the lower crust and upper mantle, following large earthquakes at the Caribbean/North America oblique subduction over the past 300 yr may contribute for 1–2 mm yr^{-1} to present-day surface displacements in eastern Hispaniola. These values are small, lower than the GPS velocity uncertainties at most

sites, and are therefore unlikely to significantly affect the results described here.

GPS velocities in Puerto Rico, St. Croix and the Lesser Antilles (Fig. 2) show that these areas move at velocities similar, in direction and magnitude, to the Caribbean plate. Slip vectors of shallow (0–50 km depth) subduction interface earthquakes in these areas parallel the Caribbean–North America relative plate motion direction. These observations indicate oblique slip—and lack of partitioning—on the Caribbean–North America subduction interface.

GPS velocities in Hispaniola show a drastically different pattern with (1) directions rotated counter-clockwise compared with the Caribbean plate motion and (2) a north–south gradient in magnitude, with velocities decreasing from the full Caribbean plate motion at the southern tip of Hispaniola to ∼2–3 mm yr^{-1} (relative to North America) along its northern coast. This pattern most likely results from elastic strain accumulation on the plate boundary faults (Calais *et al.* 2002). Earthquake slip vectors along the northern margin of Hispaniola are oriented in a trench-perpendicular direction, whereas large strike-slip faults develop in the upper plate (Septentrional and Enriquillo faults), a pattern indicative of strain partitioning (Mann *et al.* 2002).

This transition from a fully partitioned (Hispaniola) to non-partitioned (Puerto Rico) plate boundary while the plate motion obliquity remains similar coincides with the subduction of the buoyant Bahamas platform under Hispaniola. Mann *et al.* (2002) proposed that increased coupling as the buoyant Bahamas platform enters the subduction zone results in the tectonic pinning of Hispaniola, whereas Puerto Rico moves eastwards at the full Caribbean plate velocity. This interpretation requires extension between Hispaniola and Puerto Rico, consistent with GPS data (Jansma *et al.* 2000) and offshore observation of active normal faults in the Mona Passage (Grindlay *et al.* 1997; van Gestel *et al.* 1998). This oblique collision is correlated with the location of the largest

instrumentally-recorded earthquakes in the northeastern Caribbean (Dolan & Wald 1998; Russo & Villase nor 1995). It also marks the eastern termination of large strike-slip faults well developed in Hispaniola, and further west, towards Jamaica and along southern Cuba. This paper quantifies the kinematics of the northeastern Caribbean from GPS and earthquake slip vector data and discusses its implications for strain partitioning and slip rate deficit on major active faults.

2.2 Modelling approach

We model horizontal crustal velocities from GPS measurements and earthquake slip vector directions as the contribution of block rotations and elastic strain accumulation on active faults, allowing for variable interplate coupling on the subduction interface. Block boundaries and fault geometry are derived from published geological and seismological information. Model parameters (block angular velocities and fault coupling ratios) are estimated by inverting the GPS and slip vector data in a North America-fixed reference frame. We use the program DEFNODE (McCaffrey 2002, 2006), which applies the mathematical description of tectonic plate motion to smaller crustal blocks, combined with the backslip approach of Savage (1983) and the elastic half-space formulations of Okada (1992) to account for strain accumulation on block-bounding faults. DEFNODE allows faults to be partially locked by defining a coupling ratio ϕ as:

$$\phi = 1 - V_c/V,$$ (1)

where V_c is the short-term slip rate and V is the long-term (i.e. averaged over numerous earthquake cycles) slip rate. Therefore, a fault with $\phi = 0$ is fully creeping, whereas a fault with $\phi = 1$ is fully locked. Intermediate coupling ratios represent a state where the fault is partially locked. In this case, ϕ can be interpreted as the spatial average of freely slipping and locked patches (McCaffrey 2005). DEFNODE uses GPS velocities, earthquake slip vectors and fault-specific slip rates and azimuths (where applicable) and a downhill simplex minimization method to estimate the angular velocities of the crustal blocks and coupling ratio on block boundary faults.

In addition to the GPS velocities described above, we used 40 earthquake slip vectors, selecting events of magnitude greater than 5.0 that occurred on the Caribbean–North America subduction interface. Only earthquakes located in the shallow crust (above 45 km depth) are used since deeper events may represent seismicity within the slab rather than at the interface between crustal blocks. Slip vec-

tors were derived from source mechanisms from the National Earthquake Information Center database (NEIC, 2006) for events since 1977. For pre-1977 earthquakes, we used selected source mechanisms from Molnar & Sykes (1969), Calais *et al.* (1992) and Dolan & Wald (1998). Focal mechanisms for low-angle thrust events are poorly constrained by teleseismic data since the *P*-wave take off angles are much steeper than the dip of the fault plane. Molnar & Sykes (1969) also noted that the fault planes for the shallow thrust events in the northeastern Caribbean were not well determined due to the shallow dip. This uncertainty in the fault plane orientation directly affects the earthquake slip vector. Since uncertainties on source parameters are not available and given the limitations of the seismometer networks in the Caribbean and focal mechanisms using teleseismic data, we assigned a conservative uncertainty of 20° to all the events used here.

2.3 Block and fault model

The geometry of the model consists of five blocks (Fig. 3; North American Plate, Caribbean plate, Puerto Rico–Virgin Islands, central Hispaniola, Northern Hispaniola) bounded by known active faults (Northern Hispaniola Fault, Puerto Rico Trench, Lesser Antilles Trench, Septentrional Fault, Enriquillo Fault, Mona and Yuma rifts in the Mona Passage, Anegada Passage faults, Muertos Trough; Fig. 1). Fault traces and dip angles are derived from published geological and seismological information. Faults segments are divided into depth ranges, based on seismicity and changes in dip angle. Although the geometry of the major faults in the northeastern Caribbean is generally well established, some uncertainties remain, in particular for offshore faults. The faults and block boundaries are critical input to the modelling procedure and are described hereafter.

2.3.1 North Hispaniola fault and Puerto Rico trench

The North Hispaniola fault extends offshore northern Hispaniola in a roughly east–west direction. It changes to a northwesterly strike north of Cuba, where it is marked by a small trench but with no evidence for active faulting reported. Sidescan sonar and seismic reflection data offshore Hispaniola show a low angle thrust, consistent with the occurrence of a series of *M*7.2–8.1 thrust earthquakes in the 1943–1953 period to the northeast of Hispaniola (Dillon *et al.* 1992; Dolan & Wald 1998; Dolan *et al.* 1998; Grindlay *et al.* 2005b). The North Hispaniola fault is continuous to the east with the Puerto Rico trench, which shows clear evidence for low-angle
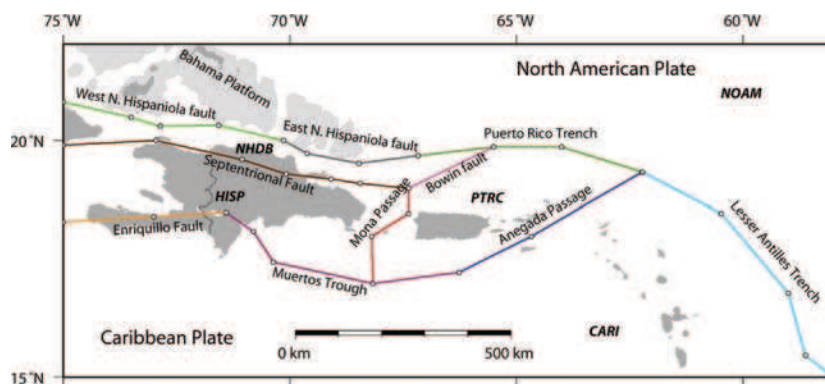
Figure 3. Block model for the northeastern Caribbean. Bounding faults shown in colour, with surface nodes indicated by open circles. Model block abbreviations are NOAM, North American block; CARI, Caribbean block; PTRC, Puerto Rican–Virgin Islands block; HISP, Hispaniola block; HDB, Northern Hispaniola Deformation block.

thrust faulting. Active strike-slip faults have also been mapped on the inner wall of the Puerto Rico trench, the most prominent of these being the Bunce and Bowin faults (Fig. 2; ten Brink *et al.* 2004; Grindlay *et al.* 2005b), which appear to connect further west with the Septentrional fault in Hispaniola. Both the North Hispaniola and Puerto Rico trench faults mark the subduction of Atlantic lithosphere beneath Hispaniola and Puerto Rico, respectively. Our geometry of the North Hispaniola and Puerto Rico trench faults is based on results by Dolan *et al.* (1998).

2.3.2 Lesser Antilles trench

The Lesser Antilles trench is the eastern margin of the Caribbean plate and the locus of subduction of Atlantic oceanic lithosphere under the Lesser Antilles active volcanic arc. It is morphologically continuous with the Puerto Rico trench to the northwest, where subduction transitions from trench-normal (Lesser Antilles) to highly oblique (Puerto Rico). The transition is marked in the upper plate by the Anegada Passage faults. We use subduction fault geometry based on seismicity studies of Stein *et al.* (1982) and Bernard & Lambert (1988), as well as profiles of NEIC catalogue seismicity from 1977–2006 (NEIC, 2006) and focal mechanisms for shallow thrust events from the Harvard/Global CMT catalogue (Ekström *et al.* 2007).

Feuillet *et al.* (2002) report active trench parallel extension in the northern half of the Lesser Antilles arc, north of about 15°N where the Tiburon Ridge is being subducted and argue that it results from strain partitioning. Lòpez *et al.* (2006) performed a detailed comparison of earthquake slip vectors and GPS velocities the same areas and report a slight difference in azimuth, possibly indicative of a crustal block separate from the Caribbean plate. We found that the discrepancies between earthquake slip vectors and GPS velocities were small and within the error limits of both data types. Also, the boundaries of a possible Lesser Antilles block are poorly defined and deformation could result from diffuse deformation within the arc rather than slip on a single fault zone, as shown by the broad distribution of mostly trench-perpendicular normal faulting within the arc (Feuillet *et al.* 2002). We therefore do not consider a separate Lesser Antilles block in our model geometry, while recognizing that a denser and more precise data set may require it.

2.3.3 Septentrional fault

The Septentrional Fault is a prominent left-lateral strike-slip fault that marks the continuation of the Oriente fault eastwards from southern Cuba. The fault trends west-northwest across northern Hispaniola for 250 km and is well expressed in submarine sonar studies both west of Hispaniola through the Windward Passage with Cuba and east of Hispaniola to the Mona Canyon (Mann & Burke 1984; Prentice *et al.* 1993; Calais *et al.* 1998; Dolan *et al.* 1998; Mann *et al.* 1998). It is also well expressed on land in the northern Dominican Republic, where it is responsible for the uplift of the Cordillera Septentrional and for active folding and faulting at its contact with late Neogene to Holocene units of the Cibao valley (Calais *et al.* 1992; Mann *et al.* 1998). Holocene slip rate on the Septentrional fault is 9 ± 3 mm yr^{-1} (Prentice *et al.* 2003), in agreement with GPS estimates (Calais *et al.* 2002).

Marine geophysical surveys north of Hispaniola (Dillon *et al.* 1992; Dolan *et al.* 1998) and Puerto Rico (Grindlay *et al.* 1997; Masson & Scanlon 1991) indicate that the Septentrional fault zone extends eastwards as far as the Mona rift, with earthquake evidence for strike-slip motion (McCann & Sykes 1984; Calais *et al.* 1992).

Further east, left-lateral strike-slip motion on the Septentrional Fault gradually merges with the Puerto Rico Trench via a series of faults that split off the main trace of the Septentrional Fault (margin-parallel thin lines on Fig. 1), including the Bunce and Bowin faults (ten Brink *et al.* 2004; Grindlay *et al.* 2005b; Mann *et al.* 2005b).

We choose a geometry with a vertical Septentrional Fault, originating west of the Windward Passage south of Cuba, extending eastwards along its mapped trace off the northern coast of Haiti, into the Cibao valley of the Dominican Republic, to the Mona Passage. From this point on, we use a shallow vertical fault that corresponds to the Bowin fault as the eastern boundary of the Northern Hispaniola Deformation block, connecting the Septentrional fault to the Puerto Rico Trench. In actuality, the transition is accommodated by several faults (as described above), and the Bowin Fault in our model is a simplification of this complex transition zone. For sake of simplicity, we use a uniform 5 km locking depth, average of the depth of the subduction interface along the fault trace. We tested different locking depths and obtained identical results, a consequence of the limited resolution due to the lack of GPS data close enough to that fault.

2.3.4 Enriquillo fault

The Enriquillo Fault is the second major left-lateral strike-slip, plate boundary-parallel, fault in Hispaniola. It is particularly well exposed in Haiti, where it is marked by a 200 km long narrow valley striking east–west through the southern peninsula (Mann *et al.* 1998). Its location has been mapped locally at the surface and in the subsurface using seismic reflection data (Mann *et al.* 1999, 1995). It is continuous to the west with the Plantain Garden fault in Jamaica, which marks the southern boundary of the eastern part of the Cayman trough, sometimes referred to as the Gonave microplate (e.g. DeMets & Wiggins 2007). The Enriquillo Fault ends abruptly in south-central Hispaniola and connects southeastwards to low angle thrust motion at the western termination of the Muertos fault (Mauffret & Leroy 1999). A number of historical earthquakes affected towns of southern Hispaniola in the 17th, 18th and 19th century, suggesting that they have occurred on the Enriquillo Fault. However, no geological estimate of slip rate is yet available for this fault.

We model the Enriquillo Fault as a single, vertical fault, originating east of Jamaica, trending eastwards into southern Hispaniola and terminating in a transition with the Muertos Trough. This transition is simplified, since there are a number of northwest-trending thrust faults mapped at the surface near the terminus of the Enriquillo Fault.

2.3.5 Muertos trough

The Muertos Trough marks the trace of a low-angle thrust fault bounding an accretionary wedge south of eastern Hispaniola and Puerto Rico (Byrne *et al.* 1985). A seismic reflection survey across the Muertos Trough, northwards to San Pedro Basin shows the structure dipping northwards at 11° to a depth of 7 km, with folded sediments on the inner trench wall suggestive of an accretionary prism (Dolan & Wald 1998). Its western terminus is believed to transition on-shore with the Enriquillo Fault, although the geometry of this transition remains unclear. This accretionary prism disappears to the east, as the Muertos thrust appears to accommodate less displacement (Jany *et al.* 1987; Masson & Scanlon 1991). Extrapolation from this depth to the location of the 1984 main shock gives

a further downdip angle of approximately 14°. The focal mechanism for the event gives a dip of 10° (Byrne *et al.* 1985), although the *SH*-wave solution differs significantly from the *P*-wave first-motion solution. Dolan *et al.* (1998) suggest a 16° dip, based on an examination of NEIC earthquake hypocentres south of Puerto Rico.

We model the Muertos fault as a steeply-dipping fault at its junction with the vertical Enriquillo Fault, rapidly decreasing to a dip of 11° (<15 km) and 16° (>15 km) as it continues eastwards towards the Mona Passage. East of the Mona Passage, the deep dip (>15 km) on our Muertos Fault increases to 27°, following the geometry from Dolan *et al.* (1998).

2.3.6 *Anegada passage*

The Anegada Passage separates Puerto Rico from the Virgin Islands and represents a complex array of normal faults and strike-slip pull-apart basins that form the Virgin Islands and Sombrero basins. There is no consensus on the role played by the Anegada Passage faults in the NE Caribbean tectonics. Interpretations range from left-lateral faulting created by interplate strike-slip motion between the Caribbean and North American plates (Mann & Burke 1984), right-lateral faulting with pull-apart basins (Jany *et al.* 1990; Masson & Scanlon 1991) and northwest–southeast rifting (Feuillet *et al.* 2002; Mann *et al.* 2005a; Speed & Larue 1991). Regardless of the style of deformation, GPS velocities from stations GORD and CRO1 located on opposite sides of the Anegada Passage show identical rates and directions within the 95 per cent confidence range, suggesting that the Anegada Passage faults accommodate only a very small fraction of the deformation across the North American–Caribbean plate boundary.

We simplify the geometry of the Anegada Passage faults as a single high-angle, through-going fault that separates the Puerto Rico and Caribbean blocks. The configuration of the Anegada Passage faults in our model links Muertos Trough with the Lesser Antilles Trench, an interpretation favoured by Masson & Scanlon (1991) and Mann *et al.* (2005a).

2.3.7 *Mona passage*

The Mona Passage, between Hispaniola and Puerto Rico, is marked in its northern part by the Mona Canyon, a steep-walled trough bounded by normal faults (Dolan *et al.* 1998). South of the Mona Canyon, a region of diffuse northwest–southeast striking normal faults continues to the southwest to near Isla Mona (Grindlay *et al.* 1997). South of Isla Mona the dominant features in the Mona Passage are two troughs, the Yuma and Cabo Rojo Canyons, interpreted by van Gestel *et al.* (1998) as north–south trending rifts. Active extension across the Mona Passage is corroborated by GPS measurements that show 2–3 mm yr^{-1} of divergence between stations in Puerto Rico and eastern Hispaniola (Jansma *et al.* 2000; Mann *et al.* 2002).

How the southern Mona Passage interacts with the Muertos Trough is not known, and whether or not the central and southern region of the Mona Passage is a boundary between the Puerto Rico and Hispaniola blocks is also not well established. However, Mann *et al.* (2005a) suggest that the Mona Canyon joins the Great Southern Puerto Rico Fault (GSPRF), effectively serving as bounding faults between the Puerto Rico and Hispaniola blocks. Grindlay *et al.* (2005a) identify several west-northwest active fault zones in the Mona Passage, the Cerro Goden, Punta Algabarrobo/Mayagez and Punta Guanajibo/Punta Areas, which merge with the GSPRF.

From here, the GSPRF trends east-southeasterly where the trace crosses southern Puerto Rico and trends offshore towards the southern extent of the Anegada Passage. Mann *et al.* (2005a) suggest that these faults help accommodate the rotation of the Puerto Rico block and that most of the strike-slip motion is accommodated by the GSPRF. However, past geological studies of traces of the GSPRF approaching the southern coastal plain do not cut post-Eocene clastic and carbonate strata, which contradicts the supposition that the GSPRF is active (Mann *et al.* 2005b). Additionally, modelling of a baseline between two continuous GPS stations that cross the Great Southern Puerto Rico Fault give a maximum fault slip rate of 1.5 ± 2.0 mm yr^{-1} (Jansma *et al.* 2000), which does not allow for significant motion across the GPS station velocities, and GPS-derived block motions support a northeastwards translation of the Puerto Rico block rather than a counter-clockwise rotation (Jansma *et al.* 2000). Thus, there is still considerable uncertainty in the southern boundary between the Puerto Rico and Hispaniola blocks.

In our model, the Mona Passage represents the largest portion of the boundary between the Puerto Rico and Hispaniola blocks. We represent the complex arrangement of normal faults throughout the Mona Passage as a single, high-angle fault, following the strike of the Mona Canyon to its southern extent, then trending southwest to Isla Mona and finally trending southwards to the Muertos Trough. This is a highly simplified geometry that is not the case in reality since sidescan sonar indicates the Muertos trough to be a continuous feature from Hispaniola to Puerto Rico (Jany *et al.* 1987), but as the southern extent of this boundary is not well constrained and in light of the lack of data for the Yuma and Cabo Rojo Canyon regions (van Gestel *et al.* 1998), we choose a model with minimal geometric complexity and parameters given the sparse geodetic coverage of the area.

2.4 Model parametrization

We discretized faults using 5×5 km rectangular patches. We found that finer (e.g. 1×1 km) or coarser (e.g. 10×5 km) grids did not improve the model fit. Given (1) the large number of estimated parameters compared to the available data; (2) the non-uniform geographic distribution of the GPS data and (3) the poor GPS coverage of the many offshore active faults, we fixed some parameters to *a priori* values and applied additional constraints to obtain a reliable solution. Optimal constraints were determined iteratively by running many models and evaluating them using the Chi-squared statistics (χ^2 and reduced Chi-squared $\chi_r^2 = \chi^2/dof$, $dof =$ degrees of freedom). We assumed uniform coupling downdip for all faults. Tests with variable downdip coupling, even when constrained to decrease linearly with depth, resulted in degraded solutions with large χ^2 and coupling uncertainties. This is a consequence of the paucity of GPS stations at close and medium distances to the subduction zones. We also equated coupling values of nodes on adjacent faults where the end nodes of these faults coincide and for neighbouring nodes for faults far from GPS data.

We fixed some faults as fully coupled where *a priori* observational data suggest these conditions to exist or where the lack of near-field GPS data do not allow for the estimation of reliable coupling coefficients. Initially, we fixed only the Septentrional and Enriquillo faults as fully coupled ($\phi = 1$), based on previous GPS results demonstrating full elastic strain accumulation on these faults and on their historical record of large earthquakes. However, we found it necessary to fix the coupling ratio of other faults at $\phi = 1$ as well, when inversion results consistently produced coupling ratios $\phi = 1$ with uncertainties greater than 1. This indicated that although the
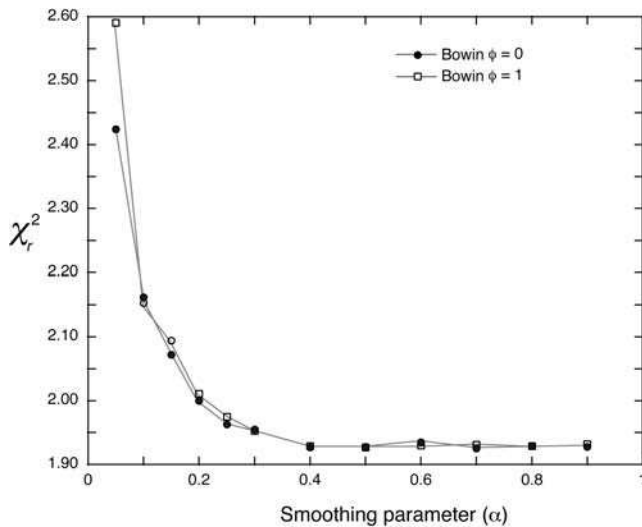
Figure 4. Reduced Chi-square χ_r^2 versus smoothing parameter. Models with $\alpha > 0.4$ have similar fit to the observational data. Models with $0.2 > \alpha > 0.4$ 0.4 show a slight increase in χ_r^2, whereas models with $\alpha < 0.2$ show a rapid increase in χ_r^2.

model preferred these faults to be fully coupled, the coupling ratio was unresolvable, given the model geometry and data distribution. We therefore fixed the coupling ratio to 1 on the Muertos Trough, Mona Passage fault, Anegada Passage fault and Bowin fault. This greatly improved the model fit to the data and lowered the coupling uncertainties on other faults, not fixed within the model.

In addition, we constrained the motion of the Caribbean plate to the angular velocity from DeMets *et al.* (2000). We tested estimating the Caribbean–North America angular velocity but found that uncertainties on the coupling parameters increased significantly, although the angular velocity estimate did not differ significantly from that of DeMets *et al.* (2000). Finally, our estimated parameters are three angular velocity parameters for each block (Northern Hispaniola, Puerto Rico-Virgin Islands and central Hispaniola) and eight coupling ratios for 132 data values (GPS velocities and earthquake slip vectors).

To regularize the solution, we apply a smoothing constraint that limits the spatial gradient of coupling along faults to a maximum value α (coupling variation per degree). Since fault nodes are spaced approximately $1°$ apart, a value of $\alpha = 1$ represents a fully undamped solution, whereas $\alpha = 0$ represents a completely damped solution. To identify the optimal smoothing parameter, we compared the model χ_r^2 for a range of values of α (Fig. 4). We find a significant decrease in the χ_r^2 as α is increased from 0.05 to 0.4. For $\alpha > 0.4$, there is essentially no change in the χ_r^2. We therefore considered a smoothing parameter of $\alpha = 0.4$ to be an optimal compromise between smoothness and model fit to the data. For the remainder of this paper, we refer to this optimal model unless otherwise indicated.

3 MODEL RESULTS

Fig. 5 shows our preferred model with a total Chi-square of 223.8 and a reduced Chi-square of 1.93. Corresponding block angular velocities are given in Table 1. Residual horizontal velocities for GPS stations (Fig. 7) are, for the most part, well within the data uncertainties (WRMS = 1.3 mm yr^{-1}) and do not show any systematic bias. Across-fault profiles showing the model fit to the GPS

data are shown in Fig. 6. The profiles show predicted profile-normal and profile-parallel displacement rates and the GPS displacement rates from stations within 60 km projected to the profile line (with the exception of profile F–F′, which had stations within 100 km projected to the profile line). GPS displacements for the most part, agree with the model within standard deviation, with the exception of a few stations within central Hispaniola. This may be due to internal deformation within the Hispaniola block, as suggested by the active uplift of the Cordillera Central.

3.1 Fault coupling ratios

Our optimal model produces a gradual decrease in the interplate coupling ratio along the Northern Hispaniola fault, from a high coupling along its western segment (from Cuba to the Dominican Republic), decreasing along the eastern segment to 0.45 ± 0.26 north of the Dominican Republic, to nearly uncoupled (0.01 ± 0.58) north of the Mona Passage. Eastward of the Mona Passage, estimated coupling at the Puerto Rico subduction is near zero as well (0.01 ± 0.58) and increases to 0.52 ± 0.35 near the transition to the Lesser Antilles subduction zone. Model coupling for the Lesser Antilles subduction zone remains low, ranging from uncoupled just south of $19°$N, to 0.55 ± 0.16 north of $15°$N, then 0.36 ± 0.23 south of that latitude.

The low coupling (<0.5) found here along most of the Caribbean–North America subduction interface in the NE Caribbean implies that less than half of the plate motion accumulates as elastic strain susceptible of being released during earthquakes. However, the uncertainties associated with the estimated coupling ratios are large, mostly because of the small and irregularly spaced GPS data set available. To further evaluate the coupling ratios produced by our best-fit model, we compare it with a forward model that uses the same block angular velocities, but fixes all faults as fully locked. The χ_r^2 of the fit to the GPS data is 3.90, compared with a χ_r^2 1.93 for our best-fit model. A one-sided *F*-test shows that the difference in χ^2 is significant at the 95 per cent confidence level. In addition, an inspection of the GPS velocity residuals (Fig. 5) for both models shows that a fully locked model produces significantly larger residuals (WRMS = 4.5 mm yr^{-1}), especially within the Puerto Rico-Virgin Islands block and in eastern Hispaniola. This test therefore shows that the GPS data do require a partially uncoupled plate interface along the eastern segment of the Northern Hispaniola Fault, the Puerto Rico Trench and the Lesser Antilles Trench.

3.2 Fault slip rates

Fault slip rates from our optimal model are summarized in Fig. 8. Model slip rates range from 19.6 to 21.7 mm yr^{-1} for the Lesser Antilles subduction zone, consistent with the imposed Caribbean–North American plate motion in rate and direction. In contrast, slip in the western portion of the model (Hispaniola, Puerto Rico, Virgin Islands) is divided among multiple faults.

Model slip rates on Northern Hispaniola Fault range from 5 to 6 mm yr^{-1} at shallow depth (0–15 km) with a slip direction consistently oriented $\sim$N30°E, almost perpendicular to the fault trace. Because of a change in the dip of the plate interface below 15 km and the merging of the Septentrional Fault along the eastern section of the Northern Hispaniola Fault, slip rates are slightly larger at depth ($\sim$12 mm yr^{-1}) with a slip direction rotated to $\sim$N65°E.

As the Northern Hispaniola Fault accommodates the shallow ($<$15 km) boundary-normal component of the oblique plate convergence west of the Mona Passage, boundary-parallel motion is
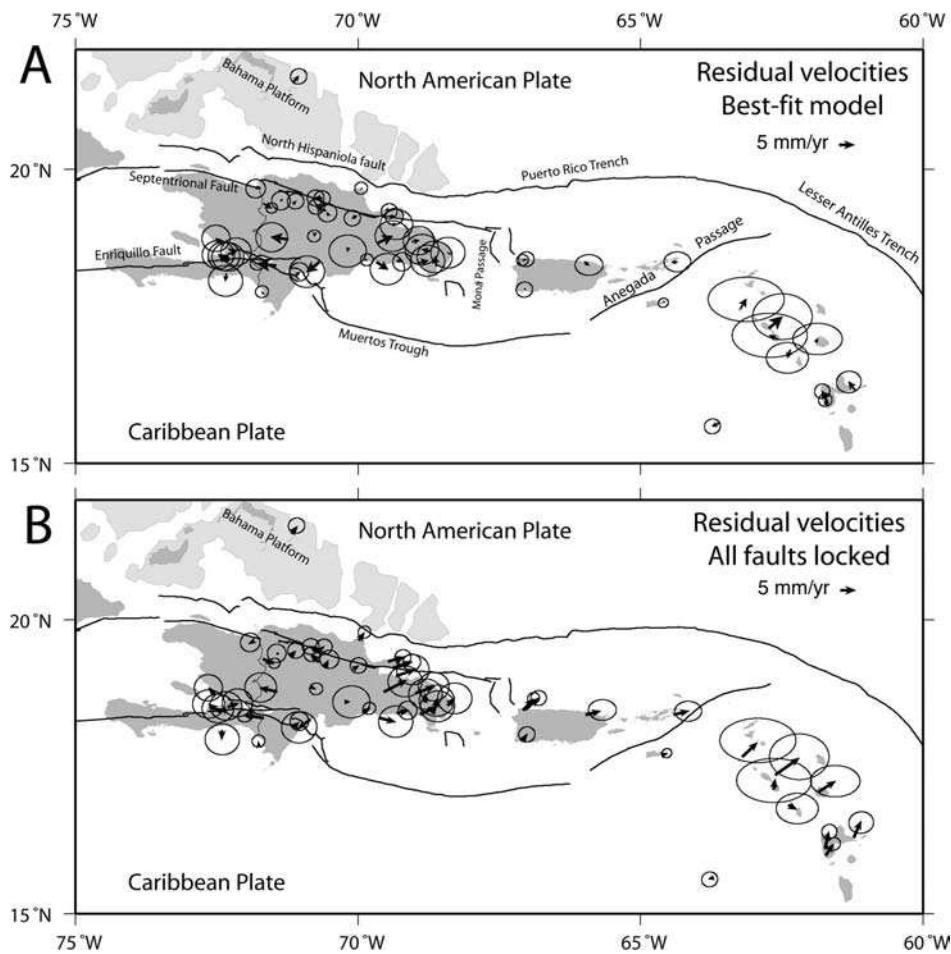
Figure 5. Fault coupling and coupling errors from the best-fit model. Open circles represent the surface projection of fault nodes. Heavy black lines show the model block boundaries. Vertical faults are shown to the right of each main figure. (a) Fault coupling for the best-fit model. Black arrows show the fault slip at mid-points between fault nodes. Grey and white arrows show observed and model velocities, respectively. (b) Coupling errors. These error estimates are strongly dependent on the data covariance and are only partially representative of the true uncertainties.

Table 1. Model angular velocity parameters for the North Hispaniola, Hispaniola, Puerto Rico and Caribbean blocks. The Caribbean rotation parameters are imposed from DeMets *et al.* (2000).

Block	Lon.	Lat.	ang.	σ_{ang}	Ω_X	Ω_Y	Ω_Z	σ_{Ω_X}	σ_{Ω_Y}	σ_{Ω_Z}
NHDB	65.78	−35.29	−0.0696	0.6960	−0.0233	−0.0518	0.0402	0.3029	0.828	0.313
HISP	59.17	−65.99	−0.1252	0.1640	−0.0261	−0.0438	0.1144	0.0923	0.2672	0.0984
PTRC	105.14	−32.56	−0.5818	0.5074	0.1281	−0.4733	0.3131	0.2143	0.4602	0.1603
CARI	70.5	−64.9	−0.214	0	−0.0303	−0.0856	0.1938	0	0	0

Note: Longitude and latitude in degrees, angular velocity (ang.) and angular velocity vector (Ω_X, Ω_Y, Ω_Z) and associated uncertainties (σ) in degree Ma^{-1}.

accommodated by the Septentrional and Enriquillo faults. Model slip rates on these two faults are 8 ± 5 and 7 ± 2 mm yr^{-1}, respectively, with left-lateral strike-slip motion. The relatively high overall uncertainty on the Septentrional Fault is due to the lack of GPS data in northern Haiti. Uncertainty decreases to 2.5–3 mm yr^{-1} further east in the Dominican Republic, where GPS data are denser. Along the Septentrional Fault, our best-fit model predicts a small additional component of extension in the Windward Passage, consistent with mapped transtensional features, and a small component of convergence in the Dominican Republic, consistent with the transpressional setting responsible for the active uplift of the Cordillera Septentrional (Calais & Mercier de Lepinay 1991). The model slip rate on the Septentrional Fault in the Dominican Republic

(8 ± 5 mm yr^{-1}) agrees well with the Holocene estimate of 9 ± 3 mm yr^{-1}, based on palaeoseismic investigations (Prentice *et al.* 2003).

Further east, model slip rate on the Bowin fault is 12.6 ± 7.6 mm yr^{-1} (left-lateral). In our models, the Bowin Fault is only purely strike-slip fault between ∼66.7°W and ∼65.5°W accommodating the plate boundary-parallel component of the Caribbean–North America oblique convergence. Kinematically, it serves to transfer left-lateral slip from the Septentrional and Enriquillo faults to the Puerto Rico Trench, with a slip rate that therefore roughly equals the sum of these two faults. Slip rate on the Bowin fault remains, however, very uncertain because of the lack of GPS data in its close vicinity. We ran additional models fixing the Bowin Fault
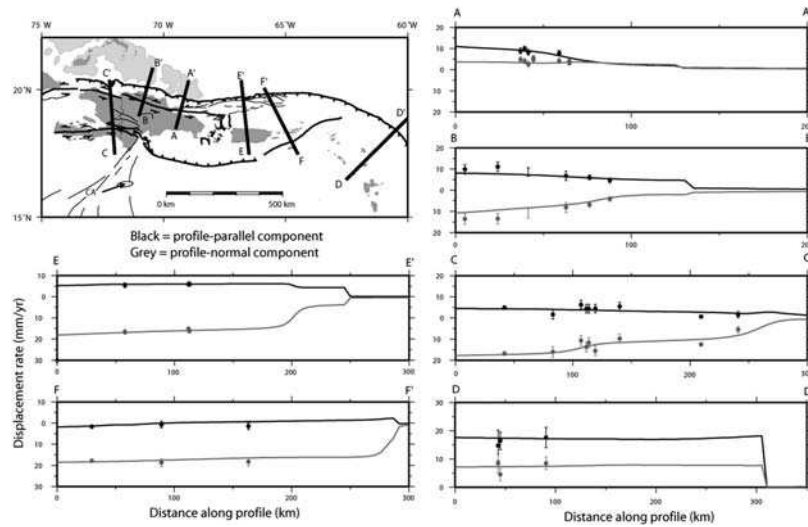
Figure 6. Cross-fault profiles showing model fit to GPS observations. For all profiles, all GPS data within 60 km are projected back to the profile line, with the exception of profile F–F′ where data within 100 km were included. Black indicates motion parallel to the profile line. Grey indicates motion perpendicular to the profile line. The solid line indicates the profile parallel/perpendicular motion produced by the best-fit model. GPS station velocity components parallel/perpendicular to the profile are shown with 1σ uncertainties. Note sparse distribution of GPS station velocities for profiles D–D′, E–E′ and F–F′.

as fully coupled or completely uncoupled and found no difference in the model results, for the same reason of a lack of near-field GPS data. Thus, the slip rate for the Bowin Fault is simply a result of a kinematic fit to the overall plate motion and fault slip budget.

Model slip rate on the Puerto Rico subduction ranges from 15 ± 3 mm yr^{-1} between 0 and 15 km, to 16 ± 3 mm yr^{-1} between 15 and 30 km and to 18 ± 2 mm yr^{-1} below 30 km depth. The slip direction is ∼N65°E, close to the N68°E direction of Caribbean plate motion with respect to North America north of Puerto Rico. Model slip rates on the Muertos Thrust average 5 ± 2 mm yr^{-1}, ranging from 7.3 ± 1.0 mm yr^{-1} west of the Mona Passage, decreasing to 1.7 ± 1.7 mm yr^{-1} east of the Mona Passage. In our model, both the Puerto Rico Trench subduction zone and the Muertos Trough accommodate oblique slip, with no partitioning of the oblique Caribbean–North America plate motion.

Finally, model slip rates on the Mona Passage fault show southwest-to-northeast extension at 5.7 ± 4.3 mm yr^{-1} trending ∼N65°E, in good agreement with previously reported extension rate of 5 ± 3 mm yr^{-1} between Hispaniola and Puerto Rico from GPS studies (Jansma *et al.* 2000; Jansma & Mattioli 2005). This extension may however involve a much broader deformation zone than modelled here, perhaps including the Bonao fault in eastern Dominican Republic (Fig. 1). Slip on the Anegada Passage fault is 3 ± 3 mm yr^{-1} directed ∼N43°W, implying northwest–southeast extension across this region. However, relative GPS velocities across the Anegada Passage are close to zero (Fig. 6, profile F–F′), suggesting that the actual slip rate may be closer to the lower end of the estimated model rate.

3.3 Slip rate deficit

The slip rate deficit d is, for each fault patch, the product of the coupling ratio ϕ and the fault slip rate s. It therefore represents the short-term deficit in slip rate compared with the secular rate and, thus, quantifies the rate at which elastic strain accumulates over a given fault area. Slip rate deficit in our best-fit model is shown on

Fig. 8. We calculate uncertainties in the slip rate deficit σ_d using

$$\sigma_d = d\sqrt{\left(\frac{\sigma_\phi}{\phi}\right)^2 + \left(\frac{\sigma_s}{s}\right)^2}, \qquad (2)$$

where σ_ϕ and σ_s are the uncertainties in coupling ratio and slip rate. Where uncertainties place the range of values of the slip rate deficit d greater than the fault slip rate s or less than zero, we truncate the uncertainties to keep the (1σ) range of the slip rate deficit within the range $0 < d < s$.

The average slip rate deficit for the western segment of Northern Hispaniola fault is 5 ± 5 mm yr^{-1}. The slip rate deficit varies with depth on the eastern segment, with averages of $1.5 + 2.8/-1.5$ mm yr^{-1} for shallow depths (<15 km) and $2.3 + 4.3/-2.3$ mm yr^{-1} for the deeper fault (>15 km). However, some nodes have a deficit as high as 5 mm yr^{-1}. The Puerto Rico Trench has an average slip rate deficit of $5 + 8/-5$ mm yr^{-1}, but this varies laterally along the fault. The largest slip rate deficit (∼13 mm yr^{-1}) occurs along the eastern segment of the Puerto Rico subduction where it transitions to the Lesser Antilles subduction. The second largest slip rate deficits occurs along the Lesser Antilles subduction between 15°–16°N (10 ± 5 mm yr^{-1}).

For the faults that we fixed as fully coupled, the slip rate deficit is obviously equal to the slip rate. However, since the coupling ratio is fixed, uncertainties in the slip rate deficit depend on uncertainties in the slip rates themselves. This gives slip rate deficits on the Septentrional and Enriquillo faults at 8.1 ± 4.9 and 7.3 ± 1.6 mm yr^{-1}, respectively. The slip rate deficit on the Muertos Trough is 5 ± 2 mm yr^{-1}, with the lowest deficit east the Mona Passage. The slip rate deficit on the Anegada Passage fault is 3 ± 3 mm yr^{-1} and on the Mona Passage faults is 5.7 ± 4.3 mm yr^{-1}.

4 DISCUSSION

4.1 Strain partitioning

The distribution of fault slip rates and directions found here show that, at the longitude of Hispaniola, slip from the surface down to
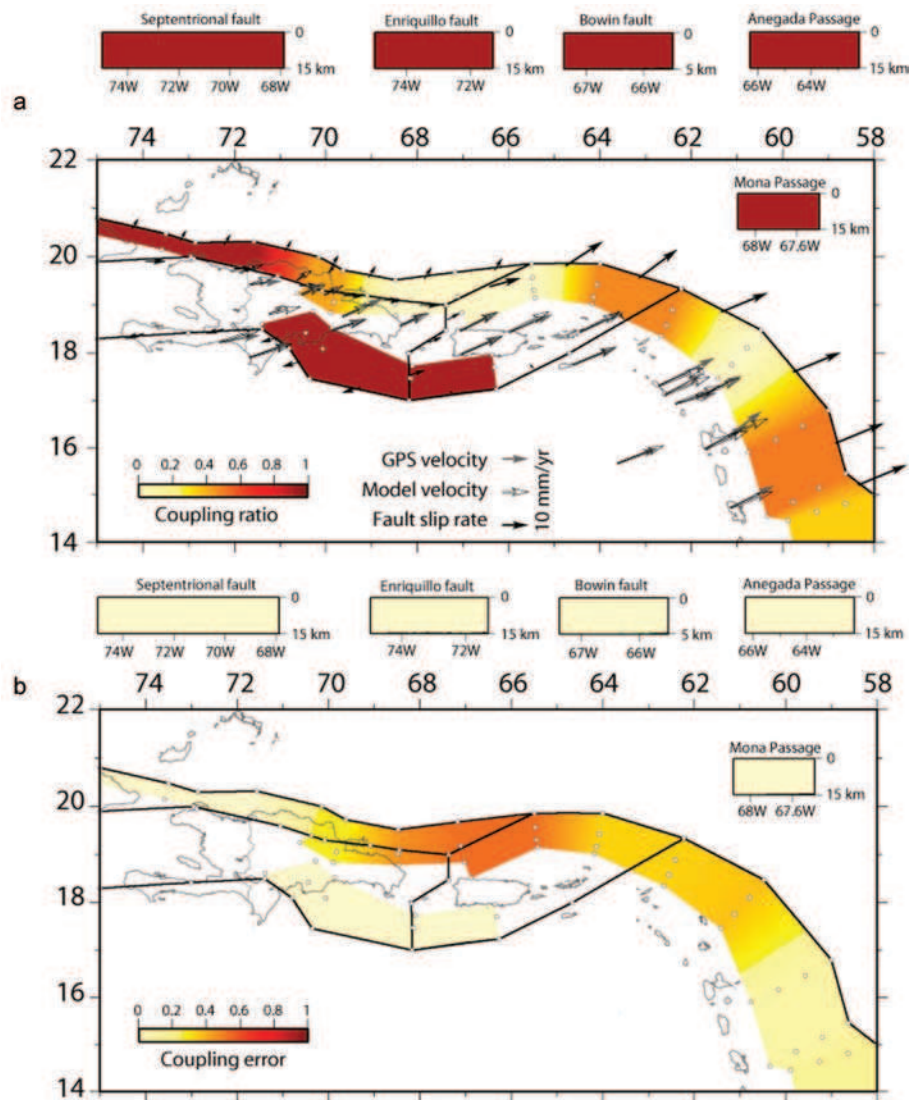
Figure 7. Model residuals for GPS velocities. (a) Black arrows, shown with 95 per cent confidence ranges, show the misfit of GPS station velocities to our best-fit model. (b) Black arrows show the misfits for a forward model that uses the same parameters as the best-fit model, except that all active faults are fully locked. Note how residual velocities increase in NE Hispaniola, Puerto Rico and the Lesser Antilles.

15 km depth is partitioned between (1) the Septentrional and Enriquillo faults, which accommodate mostly left-lateral strike-slip motion and (2) the Northern Hispaniola fault, that accommodates plate boundary-normal convergence. Combining the shallow slip rates for these faults gives a total rate of 19 mm yr^{-1} directed at N70°E, which, as expected, is equal to the Caribbean plate motion with respect to North America. Thus, GPS and earthquake slip vector data support a model of partitioning of shallow (0–15 km) slip along the northern Caribbean plate boundary, west of the Mona Passage, among the Septentrional, Enriquillo and Northern Hispaniola faults, in agreement with previous studies (Calais *et al.* 2002; Dolan *et al.* 1998).

Further east, our modelling results support the movement of a rigid (or deforming at rates lower than the current resolution of the GPS data) Puerto Rico–Virgin Islands block, rifting apart from Hispaniola at a rate of 5.7 ± 4.3 mm yr^{-1} across the Mona Passage and obliquely converging with the Caribbean plate at a rate of 1–5 mm yr^{-1} along the Muertos Trough. Fault slip on the Puerto Rico subduction is 17–20 mm yr^{-1} in a direction parallel to the

oblique Caribbean/North America plate convergence. Model results therefore show full coupling north of Hispaniola, where the oblique Caribbean/North America plate convergence is partitioned, but partial to low coupling west of the Mona Passage, where the oblique Caribbean/North America plate convergence is not partitioned, consistent with a previous analysis by ten Brink *et al.* (2004).

Chemenda *et al.* (2000) argue that strain partitioning in oblique subduction settings implies high interplate friction because friction is the main force able to drive the motion of the forearc sliver with respect to the backarc. Lateral variations in mechanical coupling along subduction zones have been interpreted as the result of differences in convergence rates and subducting plate ages (Kanamori 1983), presence of subducting sediments and seamounts (Ruff 1989; Cloos 1992), increased pore pressure due to subducted sediments (Prawirodirdjo *et al.* 1997), upper plate deformation (McCaffrey 1993), motion of the subducted slab through the mantle (Scholz & Campos 1995) and temperature of the plate interface (Hyndman & Wang 1993). The positive correlation found here between the level of interplate coupling and the degree of strain partitioning supports
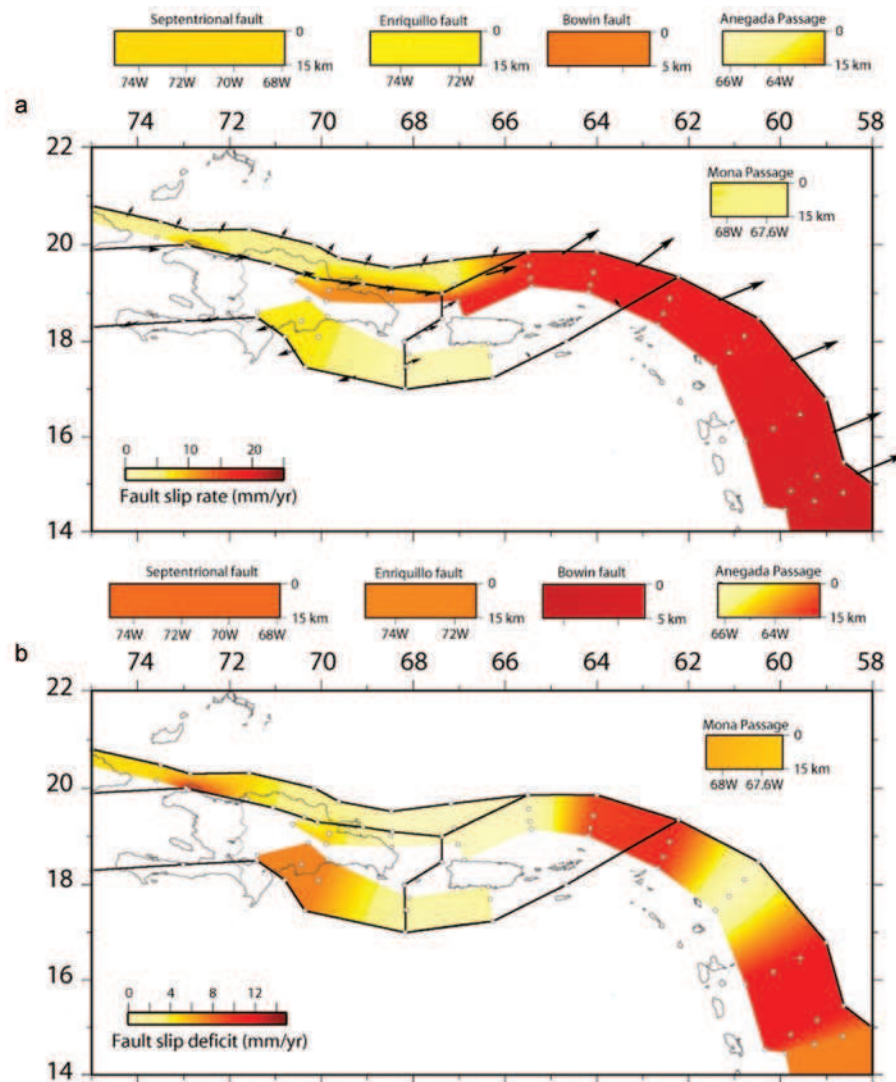
Figure 8. Fault slip rates and slip rate deficit from the best-fit model. Open circles represent the surface projection of fault nodes. Heavy black lines show the model block boundaries. Vertical faults are shown to the right of each main figure. (a) Fault slip rates (mm yr^{-1}). (b) Slip rate deficit (mm yr^{-1}).

the idea that high coupling enhances the transfer of shear stresses to the overriding plate, thereby triggering or facilitating the activation of strike-slip faulting in the backarc. The fact that the transition from strain partitioning to no strain partitioning correlates with the collisional area of the Bahamas platform with Hispaniola, suggests that the buoyant Bahamas platform acts as an asperity that mechanically couples the plate interface north of Hispaniola.

4.2 Interplate coupling

Model coupling ratios on the eastern segment of the Northern Hispaniola Fault and Puerto Rico Trench suggest that a large part of the Caribbean/North America subduction interface in the NE Caribbean is only partially locked. This is consistent with the considerable amount of microseismicity associated with the subducting North American Plate, east of the Mona Passage (Huerfano *et al.* 2005). It may be related to the subduction of an old (120 to 80 Ma from west to east), dense, oceanic lithosphere, significantly more negatively buoyant than the Bahamas platform to the west.

Since the Northern Hispaniola Fault and Puerto Rico subduction were the source of several large magnitude earthquakes during the 1943–1946 period, as well as believed to be the source of a *M*8 event in 1787 (Tanner & Shepherd 1997), the low level of coupling is surprising. However, the coupling ratios estimated here represent a spatial average for entire fault segments, which may encompass creeping areas and locked patches due to asperities (e.g. Scholz & Small 1997). In particular, the oceanic ridges entering the Puerto Rico subduction (McCann & Sykes 1984) may represent such a locked area, not resolvable spatially with the current GPS data. The low level of coupling means that the plate interface is accumulating elastic strain at rates slower than the total plate motion. This does not necessarily make it less earthquake-prone but may simply result in longer earthquake recurrence intervals compared with an equivalent, fully locked fault.

The low level of coupling found here in the source area of *M*8 earthquakes during the 1943–1946 period may also be a transient effect, as there is evidence from field, laboratory and numerical simulations that the strength of faults varies during the seismic cycle (e.g. Dieterich 1978; Scholz 1990; Rice 1992; Marone *et al.*

1995). Large earthquakes that shear fault asperities lower the frictional strength of the fault, allowing for a significant amount of creep to occur until the fault heals. Strike-slip behaviour requires a healing mechanism for faults to regain their frictional strength. Laboratory studies have shown that the static coefficient of friction increases proportional to the logarithm of contact time if two surfaces are held stationary together (Rabinowicz 1951, 1958; Scholz 2002). If the large earthquakes of the 20th century on the Puerto Rico subduction are controlled by asperities, the fault surfaces may not have recovered their frictional strength following the series of earthquakes during the 20th century, resulting in a lower level of coupling along the fault. However, the lack of well-developed strike-slip faults in the upper plate at the longitude of Puerto Rico (compared to the well-developed Enriquillo and Septentrional faults further west) indicates that the along-strike variations in partitioning and consequently, interplate coupling along the northern Caribbean plate boundary persists beyond one seismic cycle. The coupling ratios found here are therefore likely to be a long-lived feature of the plate-boundary rather than a transient effect of recent earthquakes.

Model results along the Lesser Antilles subduction also show partial coupling, with the highest degree of coupling between latitudes $15°–17°$N (slip rate deficit of 9.5 ± 5 mm yr^{-1}). This region corresponds to the intersection of the trench deformation front with the Tiburon and Barracuda ridges (e.g. McCann & Sykes 1984). The projection of these ridges downdip within the subduction zone and subsequent collision with the Lesser Antilles island arc backstop has been argued to cause elevated levels of seismicity updip of the Wadati-Benioff zone in this region, possibly responsible for the 1969 Christmas Day M6.4 earthquake and 2001 earthquake sequence (Christeson *et al.* 2003). The coincidence of this region of higher coupling with the subduction of an anomalously thick ridge suggests that subducting asperities play a significant role in the seismogenic behaviour of the plate interface.

4.3 Implications for seismic hazard

Model slip deficits can be used to calculate possible earthquake magnitudes, assuming that elastic strain accumulated since the last major earthquake on each fault was released in a single event today and the empirical scaling laws from Wells & Coppersmith (1994).

With its last major event in 1751, the Enriquillo fault in Haiti is capable of a M_w7.2 event today. The Enriquillo fault has not been investigated in detail with palaeoseismological methods and the penultimate event or a recurrence time for that fault are not known. A recurrence time of 570–710 yr is necessary to accumulate the amount of elastic strain necessary to produce an event of similar magnitude as the 1751 earthquake (M_w7.5; Tanner & Shepherd 1997).

The Septentrional fault offshore Haiti, with its latest major event in 1842, is capable of a M_w6.9 event today. A recurrence time of 1100–1250 yr is necessary to produce an event of similar magnitude as the 1842 earthquake (M_w8.0; Tanner & Shepherd 1997). Further east in the Cibao Valley of the Dominican Republic, palaeoseismological investigations along the Septentrional fault have shown that the most recent ground-rupturing earthquake occurred between AD 1040 and AD 1230 and involved a minimum of 4 m of left-lateral slip, with no major event in the past 770–960 yr (Prentice *et al.* 2003). With a model slip deficit of 8 mm yr^{-1}, the Septentrional fault in the Dominican Republic is capable of a M_w7.5 to 7.7 event. The geometry of the Septentrional fault, a single and

essentially continuous active fault trace for at least 250 km across the Cibao Valley (Mann *et al.* 1998) makes it capable of accommodating such a large earthquake. In addition, recent thrust events further north on the Caribbean–North America plate interface have increased Coulomb stresses on the Septentrional faults (Dolan & Bowman 2004; Ali *et al.* 2008). With 770–960 yr since the last major ground-rupturing earthquake and a 800–1200 yr maximum repeat time between major earthquakes (Prentice *et al.* 2003), the Septentrional fault represents a source of high seismic potential in a densely populated area of vital economical importance for the Dominican Republic.

Normal faulting within the Mona Passage is also a threat, considering the 1918 M_w7.2 earthquake and subsequent tsunami. With a slip rate deficit of ∼6 mm yr^{-1}, a recurrence time of over 300 yr is required to produce a similar event. Doubling the width of the rupture surface drops the recurrence time for a similar event to 200 yr. Large earthquakes on the Anagada Passage faults are possible, as shown by the 1867 M∼7.3 event (Fig. 1). However, the diffuse nature of faulting, combined with a low slip rate deficit, limits the recurrence time of such events to more than 500 yr.

The hazard due to large magnitude earthquakes likely increases if we consider thrust events along the plate interface. For these events, the downdip extent of rupture can extend to a depth between 30 and 60 km (Scholz 2002), resulting in an increased width of the rupture area. Thus, even with a low level of coupling, the Puerto Rico Trench may produce a $M_w > 7$ event every 100 yr due to the larger potential rupture area. If we apply this slip rate deficit over 100 yr to a 200×20 km rupture surface, this results in a M_w7 event. This would be roughly equivalent to a 50×20 km asperity that is completely coupled, accumulating slip at a full rate of 17 mm yr^{-1} over a 100-year recurrence period. Additionally, if the accumulated slip over 200 yr (based on an average slip rate deficit of 11 mm yr^{-1}) along the Lesser Antilles Trench from $15°–17°$N (200×20 km rupture) were released, it would result in a M_w7.6 earthquake. Although the Puerto Rico Trench and Lesser Antilles Trench lie several hundreds of kilometers offshore, the risk of tsunamis caused by coseismic displacements or triggered undersea landslides represents a considerable hazard in the northeastern Caribbean (LaForge & McCann 2005).

5 CONCLUSIONS

Using GPS and earthquake slip vector data, we have produced a present-day kinematic model for the northeastern Caribbean. The model accounts for secular block rotation and elastic strain accumulation, with variable interplate coupling, on active faults. We confirm that the oblique convergence between the Caribbean and North American plates in Hispaniola is partitioned between plate boundary parallel motion on the Septentrional and Enriquillo faults in the overriding plate and plate-boundary normal motion at the plate interface on the Northern Hispaniola Fault. To the east, the Caribbean/North America plate motion is accommodated by oblique slip on the faults bounding the Puerto Rico block to the north (Puerto Rico subduction) and to the south (Muertos thrust), with no evidence for partitioning. We find a positive correlation between the level of interplate coupling and the degree of strain partitioning, supporting the idea that partitioning occurs if shear stresses in the overriding plate are large enough to activate strike-slip faulting. The subduction of buoyant oceanic asperities (such as the Bahamas platform or the Tiburon ridge) probably serves to enhance the transfer of interplate shear stresses to the overriding plate.

The model slip rate deficit, together with the dates of large historical earthquakes, indicates the potential for a large (M_w7.5 or greater) earthquake on the Septentrional fault in the Dominican Republic. Similarly, the Enriquillo fault in Haiti is currently capable of a M_w7.2 earthquake if the entire elastic strain accumulated since the last major earthquake was released in a single event today. The model results show that the Puerto Rico/Lesser Antilles subduction is only partially coupled, meaning that the plate interface is accumulating elastic strain at rates slower than the total plate motion. This does not preclude the existence of isolated locked patches that are accumulating a significant amount of elastic strain to be released in future earthquakes, but may result in longer earthquake recurrence intervals compared with an equivalent, fully locked fault.

Model results suffer from a number of limitations. Most importantly, the sparse and inhomogeneous coverage of the area with GPS data results in large uncertainties on the coupling ratios and slip rates for a number of faults. This poor data coverage also limits our ability to resolve spatial variations in fault coupling ratio. Additional GPS data in Haiti and the Lesser Antilles, as well as more precise velocities in well-instrumented areas such as the Dominican Republic and Puerto Rico will help alleviate some of these issues, but the limited geographic distribution of landmass in the northeastern Caribbean will long remain a hard limit for geodetic studies. Finally, our conclusions in terms of seismic hazard do not account for the current state of stress acting on active faults in the northeastern Caribbean. However, slip rate deficit on faults from this study can be used to calculate interseismic stress loading and, together with stress changes due to historical earthquakes, derive the recent stress evolution in the NE Caribbean (Ali *et al.* 2008).

ACKNOWLEDGMENTS

REFERENCES

Ali, S.T., Freed, A.M., Calais, E., Manaker, D.M. & McCann, W.R., 2008. Coulomb stress evolution in Northeastern Caribbean over the past 250 yr due to coseismic, postseismic and interseismic deformation, *Geophys. J. Int.,* doi: 10.1111/j.1365-246X.2008.03634.x.

Altamimi, Z., Sillard, P. & Boucher, C., 2002. ITRF2000: a new release of the international terrestrial reference frame for earth science applications, *J. geophys. Res.,* **107,** 2214, doi: 10.1029/2001JB000561.

Ave Lallemant, H.G. & Oldow, J.S., 2000. Active displacement partitioning and arc-parallel extension of the Aleutian volcanic arc based on Global Positioning System geodesy and kinematic analysis, *Geology,* **28,** 739–742.

Beck, M.E., 1983. On the mechanism of tectonic transport in zones of oblique subduction, *Tectonophysics,* **93,** 1–11.

Bernard, P. & Lambert, J., 1988. Subduction and seismic hazard in the northern Lesser Antilles: revision of the historical seismicity, *Bull. seism. Soc. Am.,* **78,** 1965–1983.

Bowman, D., King, G. & Tapponnier, P., 2003. Slip partitioning by elastoplastic propagation of oblique slip at depth, *Science,* **300,** 1121–1123.

Byrne, D.B., Suarez, G. & McCann, W.R., 1985. Muertos Trough subduction–microplate tectonics in the northern Caribbean? *Nature,* **317,** 420–421.

Calais, E., Han, J.Y., DeMets, C. & Nocquet, J.M., 2006. Deformation of the North American plate interior from a decade of continuous GPS measurements, *J. geophys. Res.,* **111,** B06402, doi:10.1029/2005JB004253.

Calais, E. & Mercier de Lepinay, B., 1991. From transtension to transpression along the northern margin of the Caribbean plate off Cuba: implications for the recent motion of the Caribbean plate, *Tectonophysics,* **186,** 329–350.

Calais, E., Bethoux, N. & Mercier de Lpinay, B., 1992. From transcurrent faulting to frontal subduction: a seismotectonic study of the northern Caribbean plate boundary from Cuba to Puerto Rico, *Tectonics,* **11,** 114–123.

Calais, E., Mazabraud, Y., Mercier de Lepinay, B. & Mann, P., 2002. Strain partitioning and fault slip rates in the northeastern Caribbean from GPS measurements, *Geophys. Res. Lett.,* **29,** 1856–1859.

Calais, E., Perrot, J. & Mercier de Lepinay, B., 1998. Strike-slip tectonics and seismicity along the northern Caribbean plate boundary from Cuba to Hispaniola, in *Active Strike-slip and Collisional Tectonics of the Northern Caribbean Plate Boundary Zone,* Vol. 326, pp. 125–142, eds Dolan, J.F. & Mann, P., Geol. Soc. Am. Spec. Paper.

Chemenda, A., Lallemand, S. & Bokun, A., 2000. Strain partitioning and interplate friction in oblique subduction zones: constraints provided by experimental modeling, *J. geophys. Res.,* **105,** 5567–5581.

Christeson, G.L., Bangs, N.L. & Shipley, T.H., 2003. Deep structure of an island arc backstop, Lesser Antilles subduction zone, *J. geophys. Res.,* **104,** doi:10.1029/2002JB002243.

Cloos, M., 1992. Thrust-type subduction-zone earthquakes and seamount asperities - A physical model for seismic rupture, *Geology,* **20,** 601–604.

DeMets, C., 2001. A new estimate for present-day Cocos-Caribbean plate motion: implications for slip along the Central American volcanic arc, *Geophys. Res. Lett.,* **28,** 4043–4046.

DeMets, C. & Wiggins-Grandison, M., 2007. Deformation of Jamaica and motion of the Gonave microplate from GPS and seismic data, *Geophys. J. Int.,* **168,** 362–378.

DeMets, C., Jansma, P.E., Mattioli, G.S., Dixon, T.H., Farina, F., Bilham, R., Calais, E. & Mann, P., 2000. GPS geodetic constraints on Caribbean-North America plate motion, *Geophys. Res. Lett.,* **27,** 437–440.

Dieterich, J.H., 1978. Time-dependent friction and the mechanics of stick-slip, *Pure appl. Geophys.,* **116,** 4–5.

Dillon, W.P., Austin, J.A., Scanlon, K.M., Edgar, N.T. & Parson, L.M., 1992. Accretionary margin of north-western Hispaniola: morphology, structure, and development of the northern Caribbean plate boundary, *Mar. Petrol. Geol.,* **9,** 70–92.

Dolan, J.F. & Bowman, D.D., 2004. Tectonic and seismologic setting of the 22 September 2003, Puerto Plata, Dominican Republic earthquake: implications for earthquake hazard in northern Hispaniola, *Seism. Res. Lett.,* **75,** 587–597.

Dolan, J.F. & Wald, D.J., 1998. The 1943–1953 north-central Caribbean earthquakes: active tectonic setting, seismic hazards, and implications for Caribbean-North America plate motions, in *Active Strike-slip and Collisional Tectonics of the Northern Caribbean Plate Boundary Zone,* Vol. 326, pp. 143–170, eds Dolan, J.F. & Mann, P., Geol. Soc. Am. Spec. Paper.

Dolan, J.F., Mullins, H.T. & Wald, D.J., 1998. Active tectonics of the north-central Caribbean: oblique collision, strain partitioning, and opposing subducted slabs, in *Active Strike-slip and Collisional Tectonics of the Northern Caribbean Plate Boundary Zone,* Vol. 326, pp. 1–62, eds Dolan, J.F. & Mann, P., Geol. Soc. Am. Spec. Paper.

Feuillet, N., Manighetti, I., Tapponnier, P. & Jacques, E., 2002. Arc parallel extension and localization of volcanic complexes in Guadeloupe, Lesser Antilles, *J. geophys. Res.,* **107,** doi:10.1029/ 2001JB000308.

Fitch, T.J., 1972. Plate convergence, transcurrent faults and internal deformation adjacent to southeast Asia and the western Pacific, *J. geophys. Res.,* **77,** 4432–4460.

Grindlay, N.R., Mann, P.s. & Dolan, J., 1997. Researchers investigate submarine faults north of Puerto Rico, *Eos (Transactions),* **78,** 404p.

Grindlay, N.R., Abrams, L.J., Del Greco, L. & Mann, P., 2005a. Toward an integrated understanding of Holocene fault activity in western Puerto Rico: constraints from high-resolution seismic and sidescan sonar data, in *Active Tectonics and Seismic Hazards of Puerto Rico, the Virgin Islands, and Offshore Areas,* Vol. 385, pp. 139–160, ed. Mann, P., Geol. Soc. Am. Spec. Paper.

Grindlay, N.R., Mann, P., Dolan, J.F. & van Gestel, J.P., 2005b. Neotectonics and subsidence of the northern Puerto Rico-Virgin Islands margin in response to the oblique subduction of high-standing ridges, in *Active Tectonics and Seismic Hazards of Puerto Rico, the Virgin Islands, and Offshore Areas,* Vol. 385, pp. 31–60, ed. Mann, P., Geol. Soc. Am. Spec. Paper.

Huerfano, V., von Hillebrandt-Andrade, C. & Bez-Sanchez, G., 2005. Microseismic activity reveals two stress regimes in southwestern Puerto Rico, in *Active Tectonics and Seismic Hazards of Puerto Rico, the Virgin Islands, and Offshore Areas,* Vol. 385, pp. 81–101, ed. Mann, P., Geol. Soc. Am. Spec. Paper.

Hyndman, R.D. & Wang, K.J., 1993. Thermal constraints on the zone of major thrust earthquake failure: The Cascadia subduction zone, *J. geophys. Res.,* **98,** 2039–2060.

Jansma, P.E. & Mattioli, G.S., 2005. GPS results from Puerto Rico and the Virgin Islands: constraints on tectonic setting and rates of active faulting, in *Active Tectonics and Seismic Hazards of Puerto Rico, the Virgin Islands, and Offshore Areas,* Vol. 385, pp. 13–30, ed. Mann, P., Geol. Soc. Am. Spec. Paper.

Jansma, P.E., Mattioli, G.S., Lopez, A., DeMets, C., Dixon, T.H., Mann, P. & Calais, E., 2000. Neotectonics of Puerto Rico and the Virgin Islands, northeastern Caribbean, from GPS geodesy, *Tectonics,* **19,** 1021–1037.

Jany, I., Mauffret, A., Bouysse, P., Mascle, A., Mercier de Lepinay, B., Renard, V. & Stephan, J.F., 1987. Relevé bathymétrique Seabeam et tectonique en décrochement au sud des Iles Vierges [Nord-Est Caraibes], *C.R. Acad. Sci. Paris,* **304**(Ser. II), 527–532.

Jany, I., Scanlon, K.M. & Mauffret, A., 1990. Geological interpretation of combined Seabeam, GLORIA and seismic data from Anegada Passage (Virgin Islands, North Caribbean), *Mar. Geophys. Res.,* **12,** 173–196.

Jarrard, R.D., 1986. Relations among subduction parameters, *J. geophys. Res.,* **24,** 217–284.

Kanamori, H., 1983. Global Seismicity, in *Earthquakes: Observation, theory and interpretation*, eds Kanamori, H. & Bosch, E., pp. 597, North Holland, New York.

La Femina, P.C., Dixon, T.H. & Strauch, W., 2002. Bookshelf faulting in Nicaragua, *Geology,* **30,** 751–754.

LaForge, R.C. & McCann, W.R., 2005. A seismic source model for Puerto Rico, for use in probalistic ground motion hazard analyses, in *Active Tectonics and Seismic Hazards of Puerto Rico, the Virgin Islands, and Offshore Areas,* Vol. 385, pp. 223–248, ed. Mann, P., Geol. Soc. Am. Spec. Paper.

Lòpez, A.M., Stein, S., Dixon, T., Sella, G., Calais, E., Jansma, P., Weber, J. & LaFemina, P., 2006. Is there a northern Lesser Antilles forearc block? *Geophys. Res. Lett.,* **33,** doi:10.1029/2005GL025293.

Mann, P. & Burke, K., 1984. Neotectonics of the Caribbean, *Rev. Geophys.,* **22,** 309–362.

Mann, P., Taylor, F.W., Edwards, R.L. & Ku, T.L., 1995. Actively evolving microplate formation by oblique collision and sideways motion along strike-slip faults: an example from the northeastern Caribbean plate margin, *Tectonophysics,* **246,** 1–69.

Mann, P., Prentice, C.S., Burr, G., Pea, L.R. & Taylor, F.W., 1998. Tectonic geomorphology and paleoseismology of the Septentrional fault system,

Dominican Republic, in *Active Strike-slip and Collisional Tectonics of the Northern Caribbean plate Boundary Zone,* Vol. 326, pp. 63–124, eds Dolan, J.F. & Mann, P., Geol. Soc. Am. Spec. Paper.

Mann, P., Grindlay, N.R. & Dolan, J.F., 1999. Penrose conference report: subduction to strike-slip transition on plate boundaries, *GSA Today,* **9,** 14–16.

Mann, P., Calais, E., Ruegg, J.C., DeMets, C., Jansma, P.E. & Mattioli, G.S., 2002. Oblique collision in the northeastern Caribbean from GPS measurements and geological observations, *Tectonics,* **21,** 1057–1082.

Mann, P., Hippolyte, J.C., Grindlay, N.R. & Abrams, L.J., 2005a. Neotectonics of southern Puerto Rico and its offshore margin, in *Active Tectonics and Seismic Hazards of Puerto Rico, the Virgin Islands, and Offshore Areas,* Vol. 385, pp. 173–214, ed. Mann, P., Geol. Soc. Am. Spec. Paper.

Mann, P., Prentice, C.S., Hippolyte, J.C., Grindlay, N.R., Abrams, L.J. & La-Davila, D., 2005b. Reconnaissance study of Late Quaternary faulting along Cerro Goden fault zone, western Puerto Rico, in *Active Tectonics and Seismic Hazards of Puerto Rico, the Virgin Islands, and Offshore Areas,* Vol. 385, pp. 115–138, ed. Mann, P., Geol. Soc. Am. Spec. Paper.

Marone, C., Vidale, J.E. & Ellsworth, W.L., 1995. Fault healing inferred from time dependent variations in source properties of repeating earthquakes, *Geophys. Res. Lett.,* **22,** 3095–3098.

Masson, D. & Scanlon, K., 1991. The Neotectonic setting of Puerto Rico, *Bull. seism. Soc. Am.,* **103,** 144–154.

Mauffret, A. & Leroy, S., 1999. Neogene intraplate deformation of the Caribbean plate at the Beata Ridge, in *Caribbean Basins,* Vol. 4: Sedimentary Basins of the World, pp. 667–669, ed. Mann, P., Elsevier Science, Amsterdam, The Netherlands.

McCaffrey, R., 1991. Slip vectors and stretching of the Sumatra fore arc, *Geology,* **19,** 881–884.

McCaffrey, R., 1992. Oblique plate convergence, slip vectors, and forearc deformation, *J. geophys. Res.,* **97,** 11 953–11 966.

McCaffrey, R., 1993. On the role of the upper plate in great subduction zone earthquakes, *J. geophys. Res.,* **98,** 11953–11966.

McCaffrey, R., 2002. Crustal block rotations and plate coupling, in *Plate Boundary Zones,* Vol. 30: Geodynamics series, pp. 101–122, eds Stein, S. & Freymueller, J.T., American Geophysical Union.

McCaffrey, R., 2005. Block kinematics of the Pacific-North America plate boundary in the southwestern United States from inversion of GPS, seismological, and geologic data, *J. geophys. Res.,* **110,** doi:10.1029/ 2004JB003307.

McCann, W.R. & Sykes, L.R., 1984. Subduction of aseismic ridges beneath the Caribbean plate: implications for the tectonics and seismic potential of the northeastern Caribbean, *J. geophys. Res.,* **89,** 4493–4519.

Molnar, P. & Sykes, L.R., 1969. Tectonics of the Caribbean and middle America regions from focal mechanisms and seismicity, *Bull. seism. Soc. Am.,* **80,** 1639–1684.

Okada, Y., 1992. Internal deformation due to shear and tensile faults in a half-space, *Bull. seism. Soc. Am.,* **82,** 1018–1040.

Pollitz, F.F. & Dixon, T.H., 1998. GPS measurements across the northern Caribbean plate boundary zone: impact of postseismic relaxation following historic earthquakes, *Geophys. Res. Lett.,* **25,** 2233–2236.

Prawirodirdjo, L. *et al.*, 1997. Geodetic observations of interseismic strain segmentation at the Sumatra subduction zone, *Geophys. Res. Lett.,* **24,** 2601–2604.

Prentice, C.S., Mann, P., Taylor, F.W., Burr, G. & Valastro, S., 1993. Paleoseismicity of the North American-Caribbean plate boundary (Septentrional fault), Dominican Republic, *Geology,* **21,** 49–52.

Prentice, C.S., Mann, P., Pea, L.R. & Burr, G., 2003. Slip rate and earthquake recurrence along the central Septentrional fault, North American-Caribbean plate boundary, Dominican Republic, *J. geophys. Res.,* **108,** doi:10.129/ 2001JB000442.

Rabinowicz, E., 1951. The nature of the static and kinetic coefficients of friction, *J. appl. Phys.,* **22,** 131–135.

Rabinowicz, E., 1958. The intrinsic variables affecting the stick-slip process, in *Proceedings of the Physical Society,* **71,** 668–675, doi: 10.1088/0370-1328/71/4/316.

Rice, J.R., 1992. Fault stress states, pore pressure distributions, and the weakness of the San Andreas Fault, in *Fault mechanics and transport properties of rocks; a festschrift in honor of W.F. Brace*, eds Evans, B. & Wong, T., Academic Press, San Diego, CA, USA, pp. 475–503.

Ruff, L.J., 1989. Do trench sediments affect great earthquake occurrence in subduction zones?, *Pure appl. Geophys.,* **129,** 263–282.

Ruff, L. & Kanamori, H., 1980. Seismicity and the subduction process, *Phys. Earth planet. Inter.,* **23,** 240–252.

Ruff, L. & Kanamori, H., 1983. Seismic coupling and uncoupling at subduction zones, *Tectonophysics,* **99,** 99–117.

Russo, R.M. & Villase nor, A., 1995. The 1946 Hispaniola earthquakes and the tectonics of the North America-Caribbean plate boundary zone, northeastern Hispaniola, *J. geophys. Res.,* **100,** 6265–6280.

Savage, J.C., 1983. A dislocation model of strain accumulation and release at a subduction zone, *J. geophys. Res.,* **88,** 4984–4996.

Scholz, C.H., 1990. *The Mechanics of Earthquakes and Faulting*, 439 pp, Cambridge Univ. Press, New York.

Scholz, C.H., 2002. *The Mechanics of Earthquakes and Faulting,* 2nd edn, p. 496, Cambridge University Press, Cambridge.

Scholz, C.H. & Campos, J., 1995. On the mechanism of seismic decoupling and back arc spreading at subduction zones, *J. geophys. Res.,* **100,** 22 103–22 115.

Scholz, C.H. & Small, C., 1997. The effect of seamount subduction on seismic coupling, *Geology,* **25,** 487–490.

Speed, R.C. & Larue, D.K., 1991. Extension and transtension in the plate boundary zone of the northeastern Caribbean, *Geophys. Res. Lett.,* **18,** 573–576.

Stein, S., Engeln, J.F. & Wiens, D.A., 1982. Subduction seismicity and tectonics in the Lesser Antilles arc, *J. geophys. Res.,* **87,** 8642–8664.

Tanner, J.G. & Shepherd, J.B., 1997. Project catalogue and Seismic hazard maps, seismic hazard in Latin America and the Caribbean, *Panamerican Inst. Geographys. History,* **1,** 143p.

ten Brink, U. & Lin, J., 2004. Stress interaction between subduction earthquakes and forearc strike-slip faults: modeling and application to the northern Caribbean plate boundary, *J. geophys. Res.,* **109,** 12 310–12 324, doi:10.1029/2004JB003031.

ten Brink, U., Danforth, W., Pollonini, C., Andrews, B., Llanes, P., Smith, S., Parker, E. & Uozumi, T., 2004. New seafloor map of the Puerto Rico Trench helps assess earthquake and tsunami hazards, *Eos (Transactions),* **85,** 349–360.

van Gestel, J.P., Mann, P., Dolan, J.F. & Grindlay, N.R., 1998. Structure and tectonics of the upper Cenozoic Puerto Rico-Virgin Islands carbonate platform as determined from seismic reflection studies, *J. geophys. Res.,* **103,** 30,505–30,530.

Wallace, L.M., McCaffrey, R., Beavan, J. & Ellis, S., 2005. Rapid microplate rotations and backarc rifting at the transition between collision and subduction, *Geology,* **33,** 857–860.

Wells, D.L. & Coppersmith, K.J., 1994. New empirical relationships among magnitude, rupture length, rupture width, rupture area, and surface displacement, *Bull. seism. Soc. Am.,* **84,** 974–1002.